Bioactive Materials 50 (2025) 525–539

Contents lists available at ScienceDirect

Bioactive Materials

journal homepage: www.keaipublishing.com/en/journals/bioactive-materials

Construction of vascularized liver microtissues recapitulates angiocrine-mediated hepatocytes maturation and enhances therapeutic efficacy for acute liver failure

Liuyang Zhu [a,1], Sen Liu [b,1], Zhuangzhuang Yang [c,1], Long Yang [d], Yueyue Yang [c], Pinsheng Han [c], Yu Miao [e], Lei Lin [c], Lilin Xu [c], Yan Li [c], Xinyue Li [c], Libo Wang [e], Tianyu Zhao [e], Weiwei Wang [c], Zilin Cui [d], Ze Wang [e,***], Deling Kong [c], Zhongyang Shen [f,**], Yamin Zhang [d,*]

[a] First Central Clinical College, Tianjin Medical University, Tianjin, 300070, China
[b] Department of Pharmacology, Shenyang Pharmaceutical University, Shenyang, 110016, China
[c] State Key Laboratory of Medicinal Chemical Biology, Key Laboratory of Bioactive Materials, Ministry of Education, And College of Life Sciences, Nankai University, Tianjin, 300071, China
[d] Department of Hepatobiliary Surgery, Tianjin First Central Hospital, Tianjin, 300192, China
[e] State Key Laboratory of Druggability Evaluation and Systematic Translational Medicine, Tianjin Institute of Pharmaceutical Research, Tianjin, 300000, China
[f] Research Institute of Transplant Medicine, Organ Transplant Center, Tianjin First Central Hospital, School of Medicine, Nankai University, Tianjin, 300192, China

ARTICLE INFO

Keywords:
Liver organoid
Vascularization
Paracrine
Acute liver failure
Regenerative medicine

ABSTRACT

Liver failure poses a significant challenge for millions of patients. The use of primary human hepatocytes and the engineering of liver organoids or liver tissue provide promising solutions to mitigate the shortage of donor organs. However, insufficient vascularization and functional immaturity remain major barriers impeding optimal functional recovery after transplantation. In this study, adult stem cells derived from human liver tissues were induced to form liver organoids, which were subsequently co-cultured with vascular organoids generated from human induced pluripotent stem cells in a defined ratio to create vascularized liver microtissues. This approach successfully established a complex vascular network analogous to that found in the liver, effectively recapitulating a more physiologically relevant liver architecture. Mechanistically, this configuration promoted the structural and secretory maturation of liver organoids through paracrine signaling from the vasculature. Following transplantation into the mesentery of mice, the vascularized liver microtissues rapidly established connections with the host vasculature and enhanced secretion of albumin into the bloodstream. Moreover, the transplantation of vascularized liver microtissues could effectively ameliorate liver injury and inflammatory responses, reduce apoptosis while promoting cell proliferation in CCl_4-induced acute liver failure mice. These findings provide a robust platform for investigating the interactions between vessels and liver, and have important implications for liver failure treatment in the field of regenerative medicine.

1. Introduction

The liver is a crucial organ that plays central roles in drug metabolism, synthesis of proteins and enzymes, and glycogen storage, as well as the only solid organ in the body that possesses high regenerative capability [1]. The increasing prevalence of liver diseases caused by hepatitis virus infections, alcohol consumption, and obesity has rendered end-stage liver disease a significant global health concern [2]. Particularly, acute liver failure (ALF) can lead to severe liver damage and rapid deterioration of the condition, necessitating timely and

Peer review under the responsibility of editorial board of Bioactive Materials.
* Corresponding author.
** Corresponding author.
*** Corresponding author.
E-mail addresses: wangze9452@163.com (Z. Wang), zhyshentjfch@sina.com (Z. Shen), 5020200824@nankai.edu.cn (Y. Zhang).
[1] These authors contributed equally to this work.

https://doi.org/10.1016/j.bioactmat.2025.04.030
Received 25 December 2024; Received in revised form 4 April 2025; Accepted 23 April 2025

effective intervention [3]. Liver transplantation is still the only effective treatment option for liver failure, but it is severely limited by the shortage of donor livers, immune rejection response, and postoperative complications [4]. As an alternative therapeutic approach to liver transplantation, regenerative medicine by using autologous or allogeneic “hepatocytes" to replace damaged liver tissue or cells has made significant advancements in recent years [5]. However, utilizing hepatocytes to treat ALF in existing studies face the problems of low efficiency and failure to restore liver function over the long term. Therefore, the development of transplantable functional liver microtissues through hepatocyte engineering is a promising strategy in the field of liver regenerative medicine [6,7].

Remarkable progress has emerged in the cell and tissue engineering to construct liver microtissues [8]. Primary human hepatocytes (PHHs) are still the preferred choice for liver tissue engineering, with the enhanced hepatocyte functions in vitro and in vivo by three-dimensional culture [9]. However, it is exceedingly challenging to culture and expand PHHs while maintaining their functionality. Therefore, to acquire functional hepatocytes as seed cells in a safe and reliable manner is a major challenge of liver regenerative medicine. Liver organoids (LOs) can reproduce the specific structures and functions of the liver in vitro, thus providing a novel strategy to address the source of hepatocytes [10]. Considering the regenerative capacity of the liver and compatibility with autologous organs, LOs derived from adult stem cells (ASCs) exhibit superior adaptability and reproducibility compared to those derived from induced pluripotent stem cells (iPSCs) and embryonic stem cells (ESCs) [11]. The in vivo transplantation capability of LOs as functional hepatocytes was evaluated in some studies, which significantly improved the survival rate of mice with liver injury [12–14].

The vascular network is essential for delivering oxygen and nutrients to organs and tissues, thus the liver microtissue is desired to develop a vascular network in it that can anastomose with host blood vessels following transplantation to achieve its functionalization [15]. Co-culture of iPSCs, human umbilical vein endothelial cells and mesenchymal stem cells has been studied to generate vascularized and functional liver buds, which could connect with host blood vessels and restore liver functions after transplantation [16]. It has been indicated that endothelial cells can promote the differentiation and maturation of LOs by paracrine signaling (termed “angiocrine”) as well as their survival post-transplantation [17,18]. However, it is insufficient to reconstruct an intact vascular structure composed of endothelial cells, smooth muscle cells, or pericytes by co-culture with endothelial cells alone. Recently, vascular organoids (VOs) derived from iPSCs have been reported for the investigation of diabetic vasculopathy and they could form a complete and perfused vascular system after transplanted into mice [19,20]. Additionally, VOs have been fused with brain organoids to create vascularized brain organoids, facilitating the study of neurovascular interactions [21,22]. Therefore, it is promising to construct vascularized liver microtissues (vLMs) by co-culturing LOs with VOs.

In this study, ASCs from human liver tissues were induced to LOs with characteristics of mature hepatocytes, which were further co-cultured with iPSCs-derived VOs to generate vLMs. It was observed that the vascular networks integrated with the LOs, interconnecting the dispersed LOs into a liver microtissues that resembled the structure of liver architecture. And we demonstrated that the vasculature promotes the differentiation and maturation of LOs through paracrine signaling in vitro. After transplantation into the mesentery of mice, vLMs showed improved liver function compared with LOs and the vascular networks were able to establish connections with the host blood vessels. Furthermore, the transplantation of vLMs could significantly alleviate liver injury and inflammatory responses, reduce apoptosis while promoting cell proliferation in carbon tetrachloride (CCl_4)-induced ALF mice. These above results indicated that vLMs possess a notable therapeutic efficacy for ALF and hold great potential for clinical research in the field of liver regenerative medicine.

2. Materials and methods

2.1. Initiation, expansion, and differentiation of LOs

Liver tissues were received from patients who underwent partial hepatectomy due to liver trauma in Tianjin First Central Hospital. The Medical Ethics Committee of Tianjin First Central Hospital approved the use of these tissues for research (2020N221KY), and informed consent was obtained from all the patients.

For the initiation of organoids, a protocol modified from the previously published method was used [23]. Briefly, the liver tissues were cut into pieces of roughly 0.5–1 mm^3, washed with PBS and digested with 2.5 mg/mL collagenase IV (Solarbio, China) at 37 °C for approximately 30 min. The resulting suspension was filtered through a 70 μm cell strainer and centrifuged at 300 g for 5 min at 4 °C. After cell counting, the required cell suspension calculated based on the planting density was separated and centrifuged again. The cell pellet was resuspended in Matrigel (R&D, USA) quickly and seeded in a 24-well plate at a density of 2-3 × 10^4 cells (50 μL Matrigel) per well. After Matrigel was solidified, organoid initiating medium (OIM) was added and replaced every 3 days. Cholangiocyte organoids (COs) formed after 5–7 days and could be mechanically dissociated into fragments for passage. For the expansion of COs, organoids were collected with cold basal medium following by pipetting up and down 100 times with a p1000 tip. The samples were centrifuged and resuspended in Matrigel for seeding in plates, and the medium was substituted with organoid growth medium (OGM). Once the diameter of COs reached 300–500 μm, they could be passaged again, cryopreserved, or collected for analysis.

For the differentiation of COs into LOs, organoid differentiation medium (ODM) was added after 3 days of passage, and fresh medium was replaced every 2–3 days. Differentiated LOs could be obtained after 10 days for further analysis and subsequent experiments. The components of OIM, OGM, and ODM are listed in Table S1.

2.2. Generation of VOs from iPSCs

All experiments involving iPSCs in this study were approved by Medical Ethics Committee of Tianjin First Central Hospital. iPSCs were purchased from Cellapy biotechnology Co., LTD (Beijing, China) and maintained under feeder-free conditions in mTeSR medium (Stemcell, USA) on Matrigel-coated 6-well plates. And cells were passaged every 5 days using the ReLeSR (Stemcell, USA) and tested for mycoplasma contamination regularly.

The VOs were generated as previously described [19]. Briefly, iPSCs were disaggregated using 0.5 mM EDTA (Solarbio, China) for 3–5 min and mTeSR medium was added to terminate digestion. And the cell suspension was blown with a pipette and seeded into an ultra-low attachment six-well plate (2 × 10^5 cells per well), culturing with mTeSR medium containing 50 μM Y-27632 (Stemcell, USA). On the third day of culture, as the first day of embryoid bodies (EBs) formation, the medium was switched to DMEM/F12 (Gibco, USA) containing 2 % B27 (Thermo Scientific, USA), 1 % N2 (Thermo Scientific, USA), 12 μM CHIR99021 (Sigma-Aldrich, USA), and 30 ng/mL BMP-4 (Sigma-Aldrich, USA) to induce mesoderm differentiation. At day 5 of culture, cells aggregates were treated with DMEM/F12 containing 2 % B27, 1 % N2, 100 ng/mL VEGF-A (Novoprotein, China), and 2 μM forskolin (MedChemExpress, China) for 2 days to induce vascular differentiation, resulting in the formation of VOs composed of endothelial cells and pericytes. The VOs could sprout into vessel networks (VNs) by embedding in Matrigel and culturing with endothelial cell medium (ECM, Sciencell, USA) containing 15 % FBS (Gibco, USA), 100 ng/mL VEGF-A, and 100 ng/mL bFGF (Novoprotein, China). The differentiation medium was changed every two days and VNs were established after 7–10 days of culture.

2.3. Generation of vLMs

To explore the appropriate ratio of COs and VOs in co-culture, three ratios of COs: VOs were set: 30:1, 20:1, and 10:1. Briefly, 300 COs were fused with varying numbers (10; 15; 20) of VOs and co-cultured in 30 μL Matrigel. The COs only group and the VOs only group were used as controls. OGM containing VEGF-A (100 ng/mL) and bFGF (100 ng/mL) was added to the co-culture system to promote the growth of COs and the sprout of VOs. On the third day, the medium was replaced with ODM containing VEGF-A (100 ng/mL) and bFGF (100 ng/mL) and changed every 2 days for 10 days, during which time COs differentiated into LOs and VOs sprouted into VNs. The efficiency of organoid in forming liver lobule-like structures was quantified (number of LOs forming liver lobule-like structures/total number of LOs × 100 %), as well as the diameter and quantity of liver lobule-like structures. Additionally, the expression levels of liver-specific genes (*ALB*, *AAT*, *CYP3A4*, *HNF4A*, and *ARG1*) in each group were assessed, and human albumin (ALB) and Alpha-1-Antitrypsin (AAT) as well as the urea synthesis were measured using human elisa kit (Abcam, USA).

2.4. Generation of mLOs

To verify that VNs promote the differentiation and maturation of LOs through a paracrine mechanism [17,24,25], the secretion levels of hepatocyte growth factor (HGF), bone morphogenetic protein 2 (BMP2), tumor necrosis factor-α (TNF-α), and Wnt2 in the supernatant of the VNs culture medium were measured. Then, the supernatant of the conditioned medium was added to ODM at a ratio of 1:20 for the differentiation of COs into LOs, which was termed as mLOs. The expression levels of liver-specific genes (*ALB*, *AAT*, *CYP3A4*, *HNF4A*, G6PC, and *ARG1*) were assessed, and ALB and AAT secretion levels of mLOs were measured using ELISA. In addition, the genomic profiles of mLOs were analyzed by transcriptome sequencing.

2.5. H&E and immunofluorescence staining

The collected organoids were fixed in 4 % paraformaldehyde (PFA, Solarbio, China) for 30 min at room temperature (RT), re-suspended in 3 % agarose solution and solidified on ice, then dehydrated, embedded in paraffin, and sectioned into 3 μm. H&E staining was performed after de-waxing and rehydration. For immunofluorescence staining, the sections were de-waxed, subjected to antigen retrieval with EDTA and membrane permeabilization with 0.5 % Triton-X100, then blocked with 5 % BSA and incubated with primary antibody overnight at 4 °C. After washing in PBST, sections were incubated with secondary antibody at RT for 2 h and sealed with tablets containing DAPI after a final wash. For whole-mount staining, the samples were fixed in 4 % PFA at RT for 1 h and washed with PBST for 3 times. After permeabilizing in Triton-X100 for 30 min and blocking with 5 % BSA for 1 h at RT, the samples were incubated with diluted primary antibody at 4 °C for 48 h. After washing in PBST, samples were incubated with secondary antibody at 4 °C for 48 h and the nuclear was stained with DAPI (Solarbio, China). All images were acquired using a Total internal reflection fluorescent microscope TIRF&Thunder (Leica, Germany). A list of primary antibodies and secondary antibodies is shown in Table S2.

2.6. Assays of the liver functions of LOs

To assay glycogen storage, sections of COs and LOs were stained with Periodic acid-Schiff (PAS, Solarbio, China) following the manufacturer's instructions. For the uptake and release of indocyanine green (ICG), LOs were incubated with 1 mg/mL ICG (MedChemExpress, China) for 15 min at 37 °C with 5 % CO_2. The organoids were collected and images of ICG uptake were taken under a microscope. Then the organoids were washed gently 3 times with PBS and fresh medium was added. After incubation for 1 h at 37 °C with 5 % CO_2, images of ICG release were taken. To determine the secretion of ALB and AAT as well as the urea synthesis by LOs, the supernatant was collected and analyzed using the human elisa kit (Abcam, USA) according to the manufacturer's instructions. The activity of CYP3A4 was measured by using P450-Glo™ CYP3A4 Assay kit (Luciferin-IPA) (Promega, USA) following the manufacturer's instructions. Briefly, organoids were treated with luminogenic substrate for 2 h and the CYP3A4 enzyme activity was determined by a luminometer.

2.7. RNA extraction and qRT-PCR

Total RNA was extracted and purified using a TransZol Up Plus RNA Kit (TransGen Biotech, China) according to the manufacturer's instructions, and the quantity and quality of RNA were determined through NanoDrop spectrophotometry (Thermo Scientific, USA). Using the Transcriptor First Strand cDNA Synthesis Kit (Roche, Switzerland), RNA was reverse transcribed into single-stranded cDNA, which could be used directly for subsequent PCR in the presence of gene-specific primers. RT-qPCR was conducted using FastStart Universal SYBR Green Master (ROX, Roche, Switzerland) with a real-time PCR instrument, appropriate PCR primers, and a hydrolysis probe. GAPDH was used as a housekeeping gene for the normalization of mRNA levels. A list of the sequences of forward and reverse primers is provided in Table S3.

2.8. Transcriptome-sequencing and analysis

We collected COs and LOs at different passages derived from three individual patients. H1, H2, and H3 represented the liver tissues derived from three different patients respectively. Total RNA of organoids was extracted as described above and the high-quality RNA samples were subsequently submitted to the Sangon Biotech Co., Ltd. (Shanghai, China) for library preparation and sequencing. Sequencing libraries were generated using VAHTSTM mRNA-seq V2 Library Prep Kit (Illumina®) following manufacturer's recommendations, and index codes were added to the attribute sequences for each sample. The libraries were then quantified and pooled. Paired-end sequencing of the library was performed on the NovaSeq sequencers (Illumina, San Diego, CA). FastQC was used for evaluating the quality of the sequencing data. Clean reads were mapped to the reference genome by HISAT2 with default parameters. Gene expression values of the transcripts were computed by StringTie. DESeq2 was used to determine the differentially expressed genes (DEGs) between two samples. And the DEGs were considered as significant if P-value ≤ 0.05 and $|\text{FoldChange}| \geq 2$. Cluster analysis was preceded by principal-component analysis (PCA). The volcano map and heatmap were plotted with "ggplot2" and "pheatmap" packages in R software. Functional enrichment analyses including Gene Ontology (GO) and Kyoto Encyclopedia of Genes and Genomes (KEGG) were performed to identify which DEGs were significantly enriched in GO terms or metabolic pathways. And gene set enrichment analysis (GSEA) was performed using the R package clusterProfiler.

2.9. Flow cytometric analysis

LOs, COs, and VOs were dissociated into single cells with TrypLE solution and resuspended in staining buffer. And the cells from different kinds of organoids were incubated with BV421 mouse anti-human CD326 antibody (EpCAM, BD Biosciences, USA), FITC-conjugated Anti-alpha 1 antitrypsin antibody (AAT, BD Biosciences, USA), APC-conjugated human serum albumin (ALB, BD Biosciences, USA) antibody, and Alexa 647-labeled CD31 antibody (BD Biosciences, USA), respectively. The stained cells were quantified with BD FACSCalibur and the data were analyzed using the FlowJo software.

2.10. Animal experiments

Male BALB/c Nude mice aged 6–8 weeks were purchased from Vital

River (Beijing, China). All animal experiments have been approved by the Animal Experiments Ethical Committee of Nankai University (2022-SYDWLL-000189).

For the transplantation of VNs, five VNs were encapsulated in Matrigel and implanted as a graft onto the distal mesentery of mice to explore the survival and vascular connectivity in vivo. The mice were anesthetized with 5 % isoflurane and maintained with 2 % isoflurane. An incision approximately 1 cm was made with scissors in the lower abdomen of the mice and the small intestine and distal mesentery were exposed gently using cotton swabs. The grafts of Matrigel grafts loaded with VNs were placed on the surface of mesentery with abundant blood vessels and fixed with fibrin glue around them. After suturing the abdominal wound, the mice were placed in the cage for rewarming until recovery from anesthesia. Two weeks after transplantation, tetramethylrhodamine-conjugated dextran was injected into mice via tail vein. After 30 min, the VNs were harvested for immunofluorescence staining to evaluate the angiogenesis.

To explore the advantages of vLMs transplantation in vivo, nude mice were randomly divided into three groups according to a random number table (PHHs, LOs, and vLMs, n = 6 for each group) and experiments were performed under standard laboratory procedures of randomization and blinding. To improve the cellular content within the grafts, 500 LOs and 25 VOs were fused in 60 μL Matrigel to generate vLMs. About 500 LOs (about 2×10^5 cells) and 2×10^5 PHHs in 60 μL Matrigel were used as the control groups. Anesthesia and transplantation were performed as described above. After transplantation, blood was collected weekly from the orbit of mice and serum was isolated for the detection of human albumin level using the human ALB elisa kit (Abcam, USA). Eight weeks after transplantation, dextran was injected into mice as previously described and the grafts were collected for analysis.

To evaluate the therapeutic efficacy of vLMs transplantation in the treatment of ALF. ALF model of nude mice was induced by intraperitoneal injection of 30 % CCl_4 dissolved in olive oil at a dosage of 4 μL/g (body weight). 24 nude mice were randomly divided into four groups (n = 6 for each group). The healthy nude mice without injection of CCl_4 served as the normal group. LOs (1000 LOs in 100 μL Matrigel) or vLMs (1000 LOs and 50 VOs in 100 μL Matrigel) were implanted into nude mouse at 24 h after injection of CCl_4, respectively. The ALF model of nude mice without any implantation served as the control group. Anesthesia and transplantation were performed as described above. On the third day post-transplantation, the mice were sacrificed to collect serum and liver liver tissues. The levels of alanine aminotransferase (ALT), aspartate aminotransferase (AST), alkaline phosphatase (ALP), total bilirubin (T-Bil), and albumin (ALB) were measured using a fully automated biochemical analyzer (Mindray, China). Liver specimens were subjected to paraffin embedding and sectioning for histological analysis or immunofluorescence staining, and total RNA was extracted to assess the expression levels of genes associated with inflammation (*IL-6*, *TNF-α*, *IL-1β*, and *CXCL10*) and apoptosis (*Bax* and *Bcl2*). TUNEL apoptosis kit (Elabscience, China) and Ki67 immunofluorescence staining were used to assess the levels of apoptosis and proliferation in liver tissue. And mouse IL-6, IL-10, and TNF-α elisa kit (Elabscience, China) was used to detect the levels of inflammatory factors in the serum of mice.

2.11. Statistical analysis

All statistical analyses were performed using GraphPad Prism (version 8.3.0) and R software (version 3.6.2). Data were presented as the mean ± standard error of the mean (SEM). Single comparisons between two independent datasets were performed using an unpaired Student's *t*-test. Multiple comparisons across one variable were carried out using a one-way analysis of variance (ANOVA). Statistical significance was defined as follows: $^*P < 0.05$, $^{**}P < 0.01$, $^{***}P < 0.001$, $^{****}P < 0.0001$, ns indicates no significant difference.

3. Results

3.1. LOs were generated from human ASCs and exhibited functional features of mature hepatocytes

To obtain mature LOs from ASCs, we isolated single cells from human liver tissues and suspended the cells in Matrigel to induce bipotent cholangiocyte organoids (COs), which could be expanded and differentiated to LOs (Fig. 1A). The human ASCs embedded in Matrigel could self-assemble to form COs after culturing with organoid initiating medium (OIM) for 5–7 days, which exhibited a spherical and cystic morphology (Fig. 1B and Fig. S1A). The COs cultured with organoid growth medium (OGM) could significantly grow and expand even after freezing and thawing and could be passaged every 3–5 days in a consistent ratio of 1:4 to 1:6 by mechanical separation (Fig. 1B). After several passages, COs maintained exponential growth, ensuring adequate numbers of cells for transplantation (Fig. S1B). Immunofluorescence and flow cytometry results showed that ductal epithelial marker (EpCAM) and stem cell marker (SOX9) were highly expressed in COs, indicating their self-renewal and progenitor potential (Fig. 1C and Fig. S1D). Notably, EpCAM positive epithelial cells in COs exhibited Ki67-positive proliferative state (Fig. S1C).

After 10 days of culture with organoid differentiation medium (ODM), the bipotent COs were differentiated into LOs and the lumen of spherical cystic organoids progressively darkened, accompanied by the emergence of polygonal cells resembling mature hepatocytes (Fig. 1B and Fig. S1B). LOs were then analyzed by immunofluorescence and showed strong expression of mature hepatocyte markers, such as ALB and HNF4A (Fig. 1C). Quantitative PCR was performed for the mature hepatocyte markers (*ALB*, *CYP2E1*, *CYP3A4*, *ARG1*, *CPS1*, and *G6PC*), and the expression of those markers was significantly upregulated in LOs compared to COs and resembled that of primary liver tissues (Fig. 1D). Quantitative analysis by flow cytometry demonstrated that a relatively high efficiency of hepatocyte differentiation was achieved, with the proportion of ALB^+ cells and AAT^+ cells in LOs being 98.2 % and 85.98 %, respectively (Fig. S1E). Upon differentiation, LOs revealed more functionally mature hepatocyte characteristics. PAS staining revealed pronounced glycogen accumulation in LOs (Fig. 1E). Moreover, LOs had the ability to uptake and release ICG, which was used to characterize the function of uptake, conjugation, and subsequent release of compounds similar to hepatocytes (Fig. 1F). Additionally, the secretion levels of ALB and AAT, urea synthesis, and CYP3A4 metabolic activity were significantly increased in differentiated LOs compared with COs, comparable to the levels of PHHs (Fig. 1G). Overall, the ASCs-derived LOs exhibited functional features of mature hepatocytes.

3.2. LOs exhibited the transcriptomic profiles of mature hepatocytes

To gain a comprehensive understanding of the functional features of LOs, we next analyzed the transcriptomic profiles of LOs at different passages to further validate their mature features and genetic stability. PCA analysis displayed a clear clustering of COs (different passages of H1, H2, and H3), LOs (different passages of H1, H2, and H3), and liver tissues (Fig. 2A). The volcano plot indicated that the stem cell markers (*LGR5*) and proliferation genes (*MKI67*, *KIF18B*, and *PBK*) were upregulated in COs, while the expression of mature hepatocyte genes (*ALB*, *CYP3A4*, *C6*, *FABP*1, and *ADH1A*) was upregulated in LOs, demonstrating greater maturation of LOs (Fig. 2B). In addition, the heatmap was drawn based on the liver-specific genes as described previously [13] and LOs exhibited similar gene expression profiles to liver tissue, containing gene sets for drug metabolism (*CYP2C9*, *CYP3A4*, and *CYP4F2*), lipid metabolism (*ADH1A*, *ADH6*, and *APOH*), and well-known hepatocyte markers (*ALB*, *SERPINA6*, and *UGT2B10*) (Fig. 2C). Moreover, the upregulated genes in COs were mainly enriched in chromosome segregation, cell cycle, and DNA replication as expected, which showed the characteristics of progenitor cell in COs (Fig. S2A and S2B). And GSEA

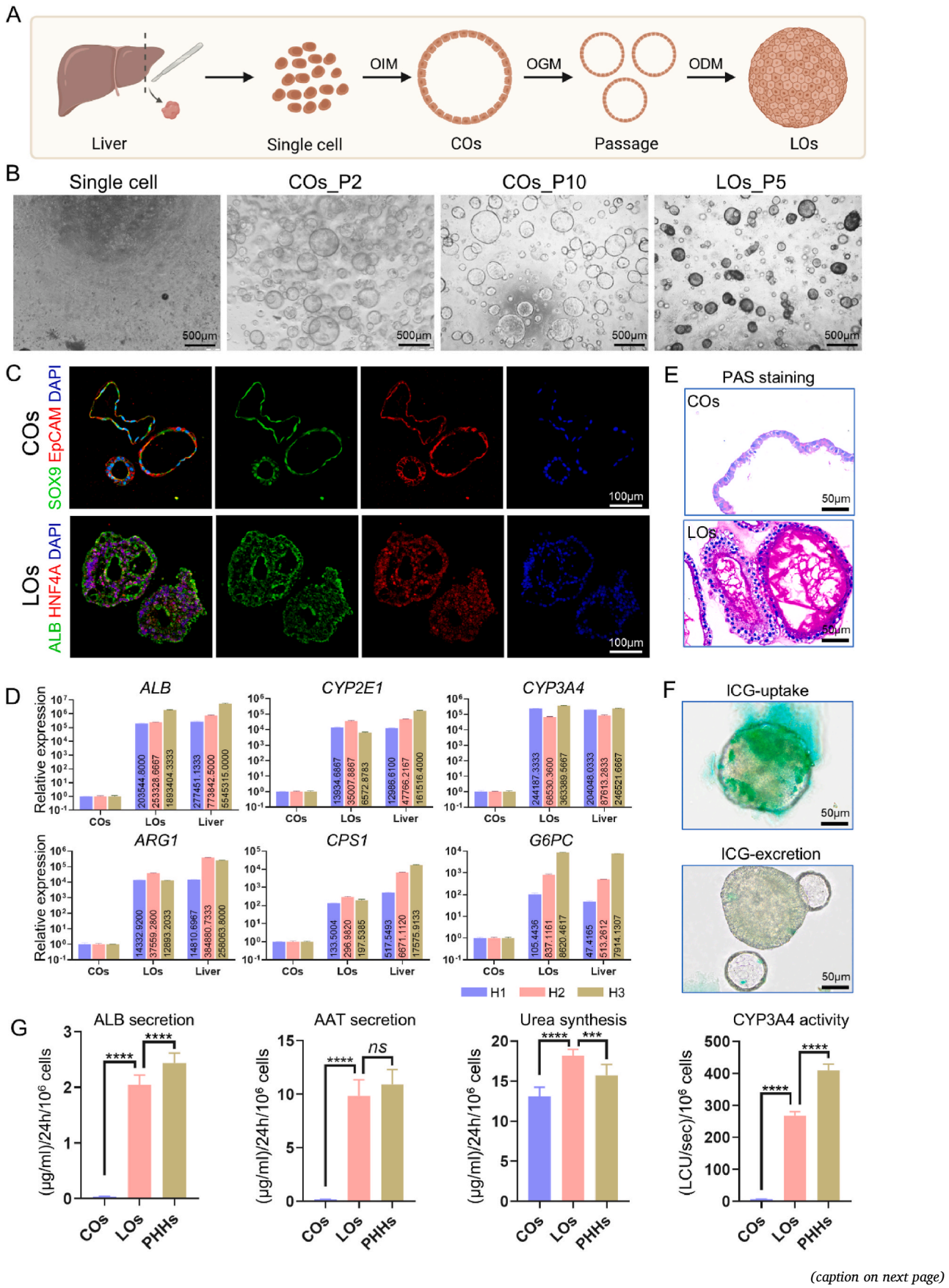

(caption on next page)

Fig. 1. Generation and characterization of LOs from human liver ASCs. (A) Schematic diagram depicting the isolation of human liver ASCs, expansion and passage of COs, and differentiation of LOs. (B) Representative images of initiation (Single cell), expansion (COs_P2, COs at Passage 2 day 3; COs_P10, COs at Passage 10 day 3) and differentiation (LOs_P5, LOs differentiated from COs at Passage 5) at different stages of LOs generation. (C) Representative immunofluorescence images of ductal epithelial marker (EpCAM) and stem cell marker (SOX9) of COs and mature hepatocyte markers (ALB and HNF4A) of LOs. (D) The relative mRNA expression levels of mature hepatocyte markers in the COs, LOs, and liver tissues. H1, H2, and H3 respectively represented liver tissues derived from three different patients. (E) Glycogen accumulation evaluated by Periodic-Acid Schiff (PAS) staining in COs and LOs. (F) Representative images of ICG-uptake and ICG-excretion of LOs. (G) Assays of the representative mature hepatocyte functions (ALB secretion, AAT secretion, Urea synthesis, and CYP3A4 activity) of LOs. COs: cholangiocyte organoids; LOs: liver organoids; OIM: organoid initiating medium; OGM: organoid growth medium; ODM: organoid differentiation medium. PHHs: primary human hepatocytes. Data are represented as mean ± SEM (n = 3). ***$p < 0.001$, ****$p < 0.0001$, ns: no significant difference.

demonstrated consistent enrichment results, confirming the high proliferation ability of COs (Fig. S2C). The GO network of upregulated genes in LOs revealed that gene sets for fatty acid, lipid, and alcohol metabolic processes, regulation of hormone levels and immune response, and small molecule biosynthetic process were enriched, which were mature functional features of liver (Fig. 2D). According to PaGenBase database [26], upregulated genes in LOs were mainly enriched in liver tissue, HEPG2 cell, and liver cell, which further indicated the hepatocyte characteristics of LOs (Fig. 2E). KEGG enrichment analysis showed that the upregulated genes in LOs were enriched in liver-related metabolic pathways, such as drug metabolism, bile secretion, and steroid hormone biosynthesis (Fig. 2F). Similarly, GSEA analysis revealed a significant enrichment of drug metabolism P450, bile acid metabolism, fatty acid metabolism, and steroid hormone biosynthesis in LOs (Fig. 2G). Taken together, transcriptomic analysis validated that LOs exhibited the molecular profiles of mature hepatocytes.

3.3. VOs were generated from iPSCs and formed functional vessel networks in vitro and in vivo

VOs were generated from iPSCs by a simplified differentiation protocol according to the previous methods [19] (Fig. 3A). Embryoid bodies (EBs) derived from iPSCs were induced to form mesoderm with CHIR99021, followed by inducing to VOs with VEGF-A and bFGF. After being embedded in Matrigel and grown in medium containing VEGF-A and bFGF for 7–10 days, VOs sprouted and endothelial cells and pericytes extending outward to assemble into VNs (Fig. 3A). PCR analysis of the different stages during VOs differentiation revealed a significant decrease in stem cell markers (*SOX2*, *OCT4*) upon VOs and VNs differentiation, whereas the vessel markers (*CD31*, *SMA*, *PDGFRβ*) showed marked increase compared to the iPSCs (Fig. 3B). The immunofluorescence of VOs showed positive expression of CD31, SMA, and PDGFRβ, suggesting that VOs were composed of endothelial cells and pericytes (Fig. 3C). Meanwhile, flow cytometry analysis revealed that the proportion of $CD31^+$ cells in the VOs reached 44.3 %, demonstrating a substantial endothelial induction efficiency (Fig. 3D).

To preserving 3D blood vessel architecture, whole-mount immunofluorescence was performed and showed that vessel-like structures sprouted out from the VOs, implying the formation of VNs. And VNs exhibited a highly branched and connected $CD31^+$ endothelial network that was covered by $PDGFR\beta^+$ and SMA^+ pericytes. Meanwhile, active angiogenesis occurred at the periphery of the vascular sprouting, where endothelial cells showed a characteristic tip cell morphology (Fig. 3E). To test whether VNs could form functional blood vessels in vivo, VOs embedded in Matrigel for 10 days were transplanted on the distal mesentery of nude mice. Two weeks later, immunofluorescence staining showed that VNs survived in vivo and $hCD31^+$ endothelial cells formed stable vascular networks. Dextran perfusion indicated that blood vessels of VNs had functionally connected to the mouse vasculature (Fig. 3F). The above results indicated that VOs derived from iPSCs faithfully recapitulated the structure and function of blood vessels and had potential for vascularization of LOs.

3.4. VOs fused with LOs to form vLMs with liver lobule-like structures

In view of the remarkable potential of VOs for vascularization, we attempted to fuse VOs with COs to construct vLMs. First, the optimal ratio of COs to VOs in the co-culture system was explored (Fig. 4A). It could be observed that VOs sprouted into VNs while LOs differentiated after fusion, which formed liver microtissue that resembled the structure of liver lobules (Fig. S3A). The statistical results showed that the formation efficiency and quantity of liver lobule-like structures in the groups of 20:1 and 10:1 were significantly higher than those in the group of 30:1 (Fig. S3B and S3D), but there was no significant difference in the diameter of the liver lobule-like structures among the three groups (Fig. S3C). The PCR results indicated that compared with COs and VOs groups, the expression of mature hepatocyte genes (*ALB*, *AAT*, *CYP3A4*, HNF4A, and *ARG1*) was significantly upregulated in all co-culture groups with different ratios. And the 20:1 group showed the most obvious up-regulation trend, although there was no significant difference in *HNF4A* expression between 20:1 group and 10:1 group, and in *ARG1* expression among the three groups (Fig. 4B). It should be pointed out that the decreased expression of mature hepatocyte genes in the 10:1 group compared with the 20:1 group may be attributed to the interference of the excessive presence of VNs-derived RNA in the co-culture system. Meanwhile, the liver function analysis showed that the secretion levels of ALB and AAT in the groups of 20:1 and 10:1 were significantly higher than those in the other groups, but there was no significant difference between these two groups (Fig. S4).

In summary, the co-culture of COs with VOs at the ratio of 20:1 and 10:1 could both efficiently generate mature and functional vLMs, but considering LOs was the principal component of vLMs, so the ratio of 20:1 was more suitable to generate vLMs. And under this condition, the scattered LOs were enveloped and connected by VNs (Fig. 4C). The whole-mount immunofluorescence further demonstrated that $CD31^+$ endothelial cells fused with $HNF4A^+$ LOs to form vLMs (Fig. 4D). Meanwhile, the levels of ALB and AAT secretion as well as urea synthesis during the differentiation process of vLMs were significantly higher than those of LOs (Fig. 4E), indicating that VOs promoted the differentiation and maturation of LOs in vLMs.

3.5. VNs promoted the differentiation and maturation of LOs through paracrine signaling

Previous studies have shown that endothelial cells can promote the maturation and proliferation of hepatocyte by paracrine signaling [17,24]. Accordingly, we hypothesized that the promotion of VNs on LOs differentiation and maturation may be mediated through high levels of paracrine factors and the supernatant of VNs was added to the ODM to induce COs differentiation into mLOs (Fig. 5A). First, ELISA was performed to detect the content of paracrine factors in the supernatant of VNs (Fig. 5B and S5). The results showed that VNs were capable of secreting sufficient levels of HGF (6.56 ± 0.125 ng/mL), with concentrations reaching equivalent levels as those added in ODM (Table S1). In addition, TNF-α and BMP2 could also be detected in the supernatant, which play important roles in hepatocyte maturation [25,27]. Then, the expression levels of mature hepatocyte genes (*ALB*, *AAT*, *CYP3A4*, HNF4A, *G6PC,* and *ARG1*) were significantly increased in the generated mLOs (Fig. 5C and S6). In addition, the secretion levels of ALB and AAT in mLOs were significantly higher than those in LOs (Fig. 5D). These results suggested that VNs-derived cytokines cocktail may promote the differentiation of LOs through paracrine signaling.

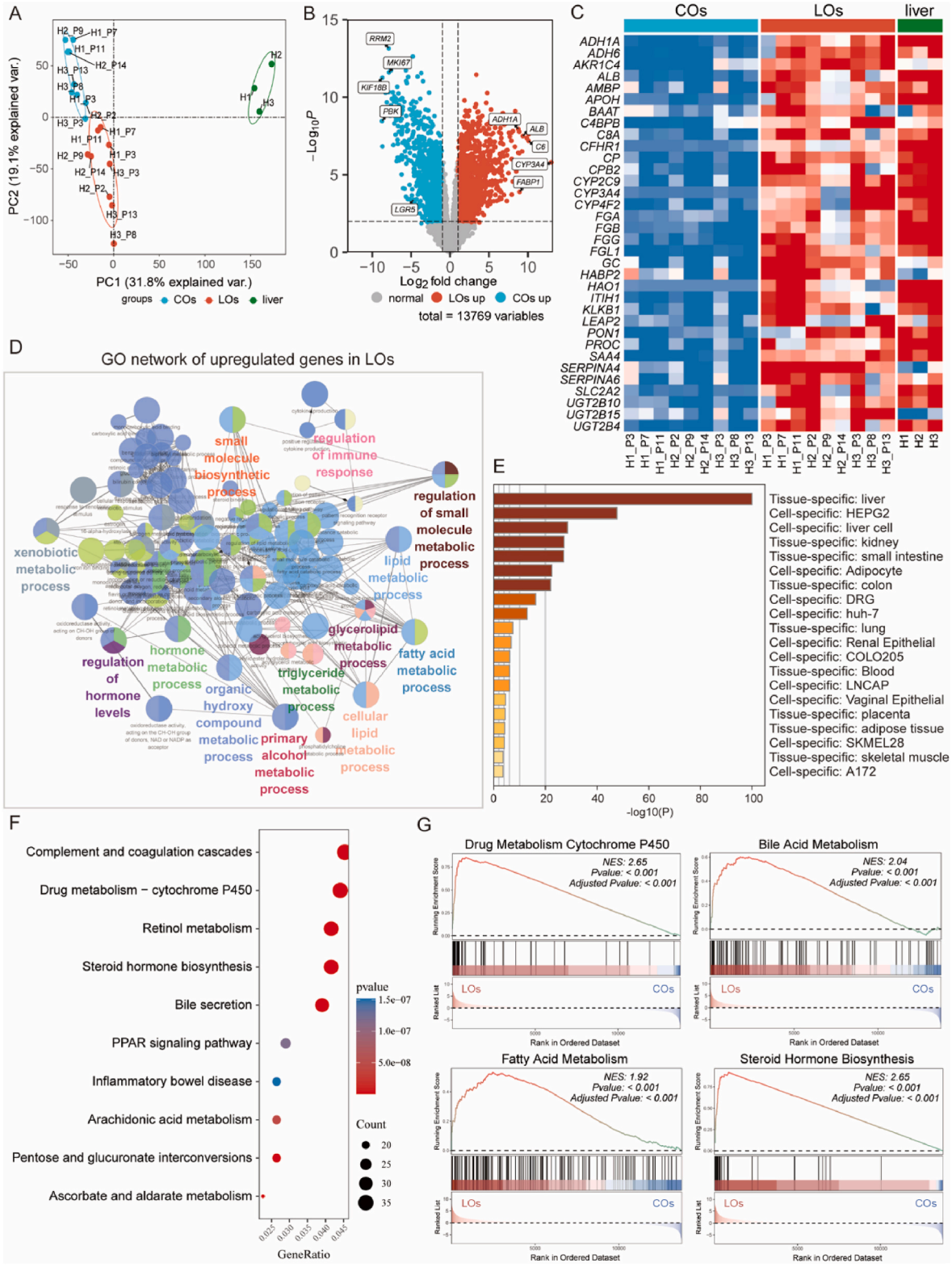

Fig. 2. Transcriptome profiles of LOs from human ASCs. (A) PCA analysis of COs (n = 9, different passages), LOs (n = 9, LOs differentiated from COs at different passages), and liver tissues (n = 3) based on global gene expression profiles. H1, H2, and H3 respectively represented liver tissues derived from three different patients. (B) Volcano plot of the DEGs in COs and LOs. (C) Heat map of liver-specific genes in COs, LOs, and liver tissues. (D) GO network of upregulated genes in LOs. (E) Enrichment analysis of upregulated genes in LOs based on PaGenBase. (F) KEGG enrichment analysis of upregulated genes in LOs. (G) GSEA analysis of hallmark pathways in LOs. COs: cholangiocyte organoids; LOs: liver organoids.

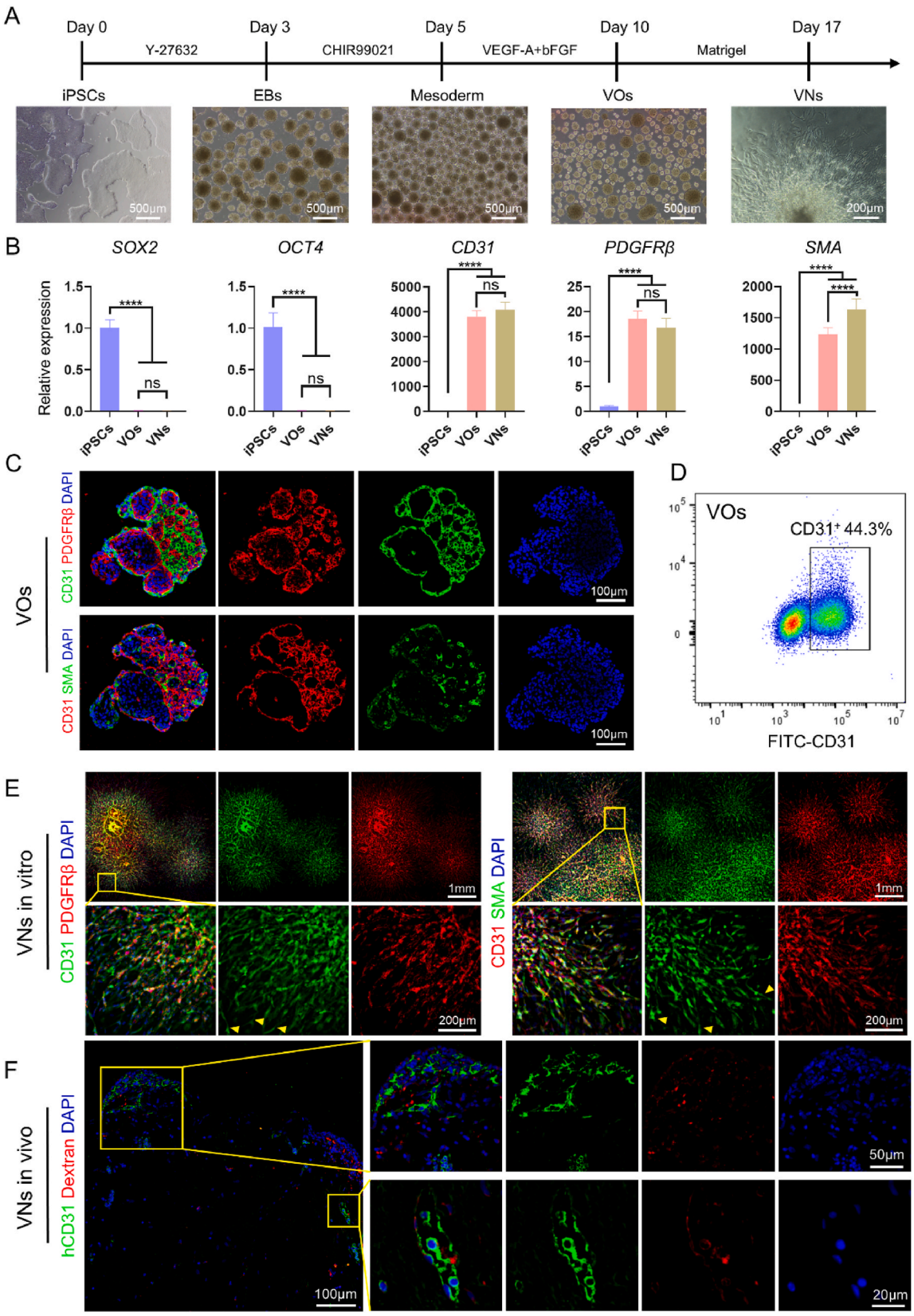

Fig. 3. Generation and characterization of VOs induced from iPSCs. (A) Schematic diagram of the timeline for generating VOs from iPSCs. (B) The relative mRNA expression levels of genes associated with stem cell and vessel markers in the iPSCs, VOs, and VNs. (C) Representative immunofluorescence images of VOs stained with vessel markers (CD31, PDGFRβ, and SMA). (D) FACS analysis to determine the proportion of $CD31^+$ endothelial cells in VOs. (E) Representative whole-mount staining of VNs. Tip cells at the periphery of sprouting vascular networks were marked by arrowheads (yellow). (F) Representative immunofluorescence images of VNs in vivo. Injection of tetramethylrhodamine-conjugated dextran (red) into mice via tail vein to mark blood vessels. EBs: embryoid bodies; VOs: vascular organoids; VNs: vessel networks. Data are represented as mean ± SEM (n = 3). ****$p < 0.0001$, ns: no significant difference.

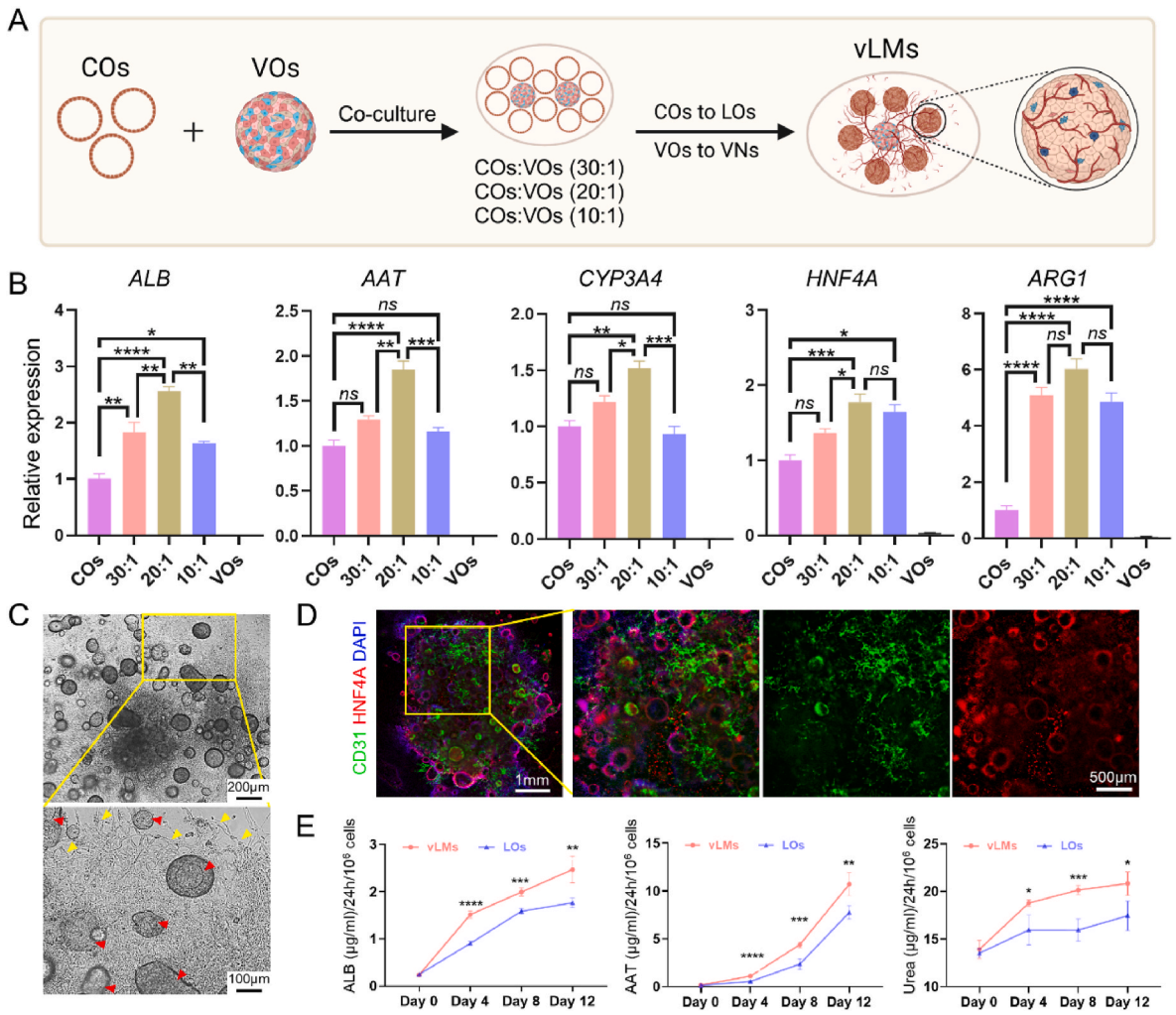

Fig. 4. Generation of vLMs with improved maturation of LOs. (A) Schematic diagram of generating vLMs by co-culture of COs with VOs at different ratios, during which time COs differentiated into LOs and VOs sprouted into VNs. (B)The relative mRNA expression levels of mature hepatocyte genes in different groups. (C) Representative images of vLMs morphology (COs: VOs = 20: 1). LOs and VNs were marked by red and yellow arrowheads, respectively. (D) Representative immunofluorescence images of vLMs (COs: VOs = 20: 1) stained with CD31 and HNF4A. (E) Quantitative analysis of ALB secretion, AAT secretion, and Urea synthesis during the differentiation period of LOs and vLMs (COs: VOs = 20: 1). VOs: vascular organoids; VNs: vessel networks; COs: cholangiocyte organoids; LOs: liver organoids; vLMs: vascularized liver microtissues. Data are represented as mean ± SEM (n = 3). *$p < 0.05$, **$p < 0.01$, ***$p < 0.001$, ****$p < 0.0001$, ns: no significant difference.

Transcriptome sequencing was performed on LOs and mLOs, and the results confirmed that mLOs exhibited enhanced hepatocyte features. PCA analysis showed the obvious differences between LOs and mLOs (Fig. 5E), and volcano plot indicated that the expression of some liver-specific genes (*FABP1*, *FABP2*, *UGT2B17*, and *SERPINB3*) was upregulated in mLOs (Fig. 5F). GO enrichment analysis showed that the upregulated DEGs in mLOs were mainly related to lipid transport, carboxylic acid transport, vascular process in circulatory system, regulation of hormone secretion, and other GO terms (Fig. 5G). KEGG enrichment analysis of the upregulated genes in mLOs showed that they were significantly enriched in bile secretion, Wnt signaling pathway, TGF-β signaling pathway, fat digestion and absorption and PPAR signaling pathway (Fig. S7). Similarly, GSEA revealed that gene expression in mLOs was predominantly enriched in the PPAR signaling pathway, TGF-β signaling pathway, Wnt signaling pathway and Starch and sucrose metabolism (Fig. S8). Heat maps indicated that the genes related to lipid metabolism, bile secretion, lipid transport, regulation of hormone secretion, and vascular process in circulatory system were upregulated in mLOs (Fig. 5H). All these results confirmed that VNs indeed promoted differentiation and functional maturation of LOs through paracrine signaling.

3.6. vLMs showed enhanced liver functions in vivo and established connections with recipient vasculature

To verify the advantages of vLMs as functional liver microtissues for implantation in vivo, vLMs, LOs, and PHHs were transplanted into the distal mesentery of nude mice (Fig. 6A). At 8 weeks after transplantation, it was observed that all the grafts had integrated into the mesentery, and there was a clear distribution of vascular networks across the surface of vLMs grafts (Fig. 6B). The samples were collected and sectioned to analyze the effect of transplantation. It was observed that the grafts in all three groups could survive for a long time in vivo and remain integrity for a certain degree, and the grafts of vLMs group exhibited a more compact tissue morphology (Fig. S9). And immunofluorescence showed that the $hALB^+$ hepatocytes in vLMs group had a significantly higher ratio than that in LOs group and PHHs group, with a distribution of cord-like pattern, indicating that the vascularization enabled vLMs to achieve a higher hepatocyte survival (Fig. 6C).

In addition to viability, vascularization was also crucial for maintaining the functionality of grafts in vivo. It was observed that the $hCD31^+$ endothelial cells within the graft of vLMs exhibited a cross-distribution with the ALB^+ hepatocytes and formed vessel-like tubular

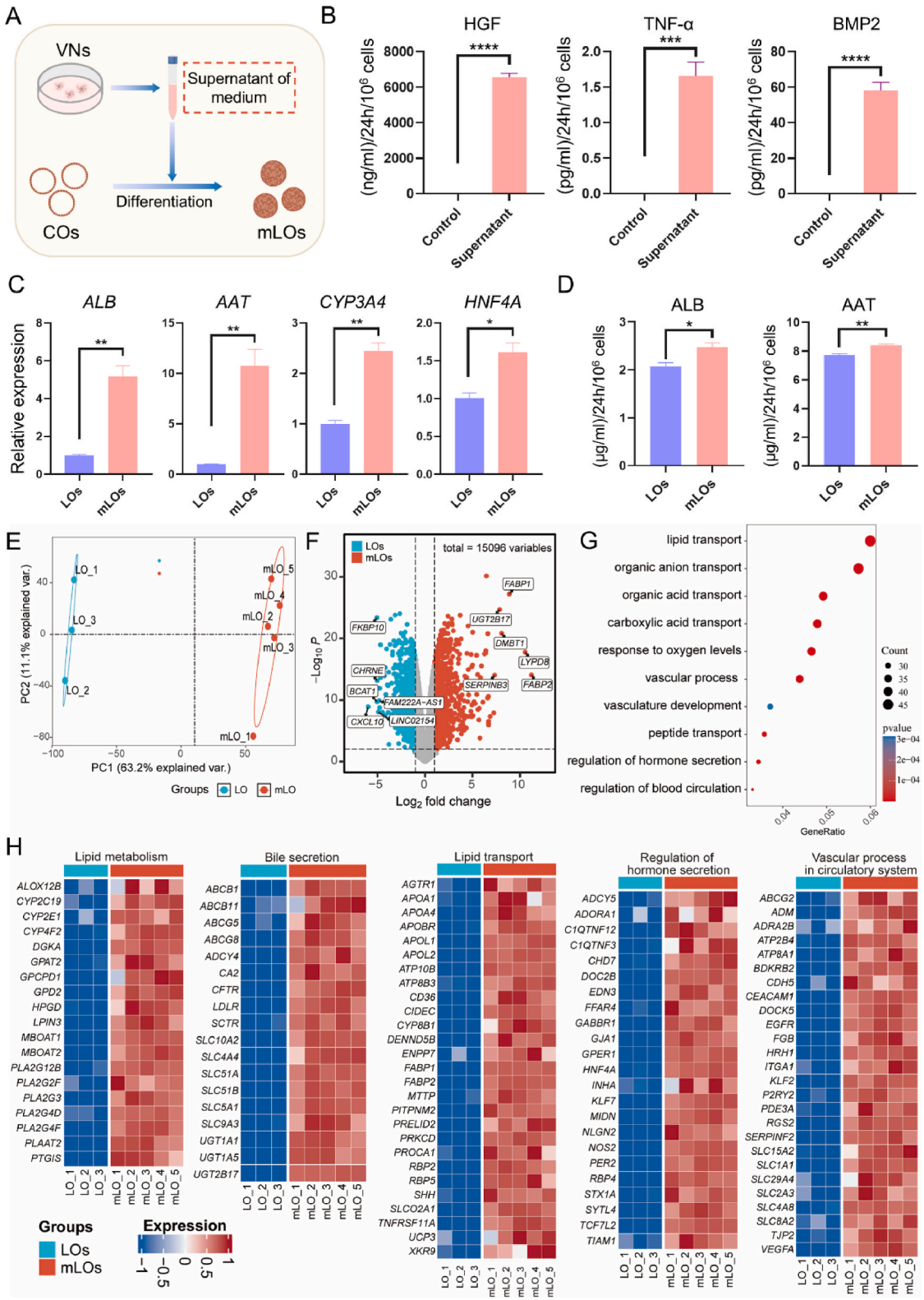

Fig. 5. VNs promoted the differentiation and maturation of LOs through paracrine mechanism. (A) Schematic diagram of generating mLOs to explore the effect of paracrine on LOs differentiation. (B) The content of paracrine factors secreted by VNs in the supernatant of medium. (C) The relative mRNA expression levels of mature hepatocyte genes in mLOs. (D) Quantitative analysis of ALB and AAT secretion in mLOs. (E) PCA of LOs and mLOs based on gene expression profiles. (F) Volcano plot of the DEGs in LOs and mLOs. (G) GO enrichment analysis of upregulated DEGs in mLOs. (H) Heat maps of genes related to lipid metabolism, bile secretion, lipid transport, regulation of hormone secretion, and vascular process in circulatory system in LOs and mLOs. VNs: vessel networks; COs: cholangiocyte organoids; LOs: liver organoids; mLOs: LOs cultured with conditioned medium of VNs. Data are represented as mean ± SEM (n = 3). *$p < 0.05$, **$p < 0.01$, ***$p < 0.001$, ****$p < 0.0001$.

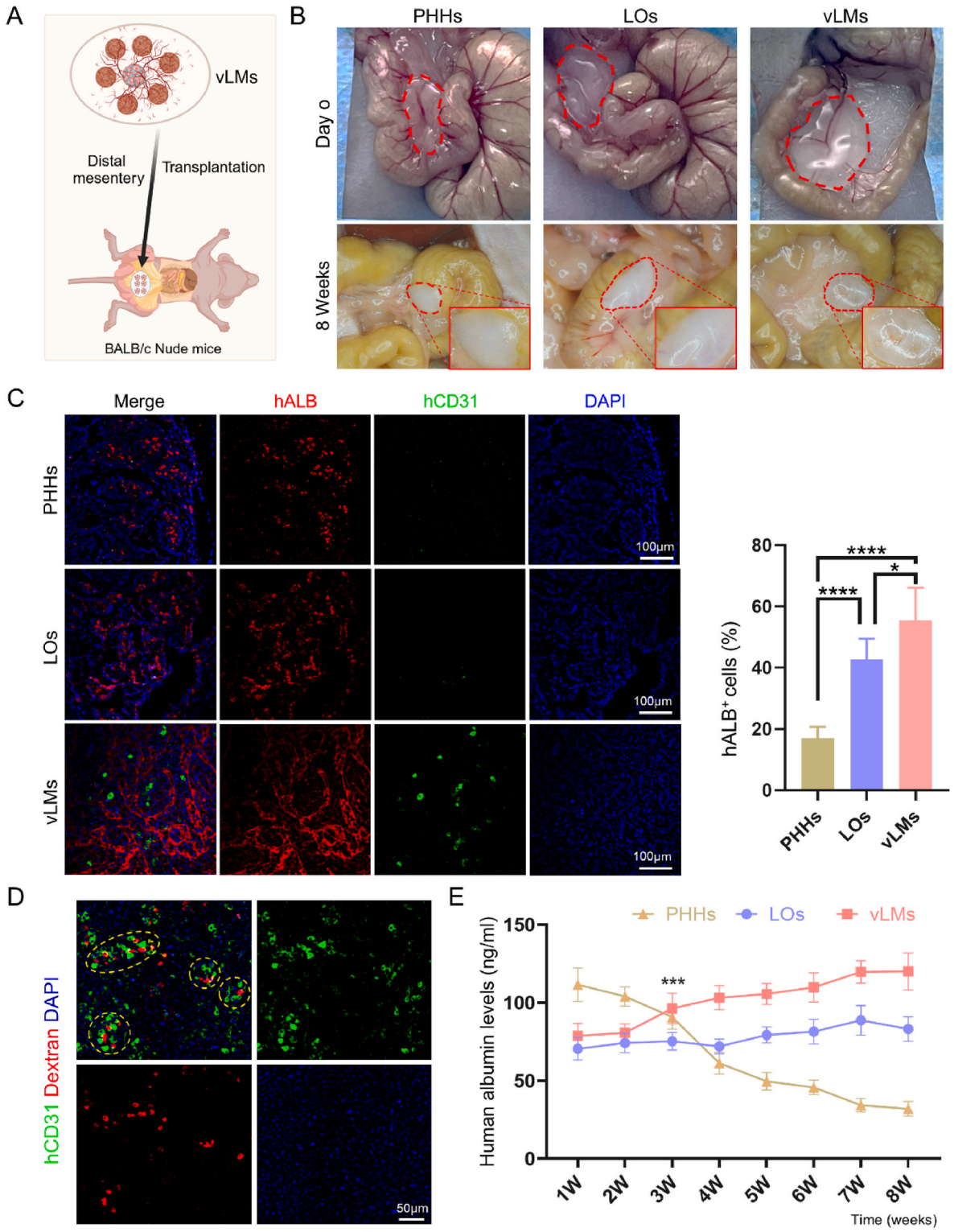

Fig. 6. Functional analysis of vLMs after transplantation in vivo. (A) Schematic diagram of vLMs transplanted into the mesentery of nude mice. (B) The macroscopic observation of PHHs, LOs, and vLMs just after transplantation into the mesentery and 8 weeks after transplantation. The sites inside the red dashed line represents where the grafts were transplantated. (C) Representative immunofluorescence images of grafts stained with hALB and hCD31 and quantification of the ratio of $hALB^+$ cells in PHHs, LOs, and vLMs. (D) Representative immunofluorescence images of vLMs grafts stained with hCD31. Injection of tetramethylrhodamine-conjugated dextran (red) into mice via tail vein to mark blood vessels. The vascular structures are delineated within the yellow dashed lines. (E) Trends of human albumin levels in recipients with transplantation of PHHs, LOs, and vLMs. PHHs: primary human hepatocytes; LOs: liver organoids; vLMs: vascularized liver microtissues. Data are represented as mean ± SEM (n = 3). $^*p < 0.05$, $^{***}p < 0.001$, $^{****}p < 0.0001$.

structures (Fig. 6C and D). The presence of the intravenous fluorescein-conjugated dextran within the graft proved the establishment of vascular connectivity between the graft and recipient in the vLMs group (Fig. 6D). To evaluate the liver function of vLMs in vivo, the secretion of human ALB in recipient mice was measured and it was found that the level of ALB in vLMs and LOs groups gradually increased and sustained for more than 8 weeks. Notably, the level of ALB in the vLMs group was significantly higher than LOs group in the third week. Although the human albumin levels in PHHs group were higher in the early stages of transplantation, it gradually declined and fell lower than those in the LOs group and the vLMs group after 4 weeks (Fig. 6E). Moreover, some $hALB^+$ cells within the vLMs exhibited higher ratio $Ki67^+$ as well, a marker of cell proliferation, indicating that the vLMs maintains proliferative activity in vivo (Fig. S10). In summary, the vascularized microenvironment of vLMs enables it to maintain good viability, activity and function in vivo.

3.7. Therapeutic efficacy of vLMs transplantation for ALF

Given that the vLMs exhibited enhanced liver functions vascular connectivity in vitro, we further evaluated their therapeutic effect in the treatment of CCl_4-induced ALF after transplantation in vivo (Fig. 7A). It was observed that the liver of ALF in control group exhibited a diffuse distribution of white nodules, whereas those in the treatment group displayed a smooth surface with a darker color. And the liver in vLMs group displayed a morphology with more uniform deep brown color compared with the LOs group, which was more similar to that of normal group (Fig. 7B). Correspondingly, the results of H&E staining revealed extensive areas of tissue necrosis in the liver of control group. Three days after transplantation, the necrotic area was significantly reduced, particularly in the vLMs group, which exhibited the least degree of liver necrosis (Fig. 7C). The biochemical analysis of mice serum indicated that the levels of ALT, AST, ALP, and T-Bil in LOs and vLMs groups were significantly decreased on the third day after transplantation, and the ALB level in vLMs group was significantly increased. Notably, the vLMs group exhibited a more pronounced recovery of liver function compared with the LOs group (Fig. 7D). The above results demonstrated that the transplantation of vLMs could alleviate the liver damage in ALF mice, demonstrating superior therapeutic efficacy.

In addition, the cell apoptosis and proliferation in the liver tissues were evaluated through Tunel and Ki67 staining, respectively. The results showed that there were fewer $Tunel^+$ cells and more $Ki67^+$ cells in vLMs group than control group and LOs group (Fig. 7E and F), indicating that the transplantation of vLMs had a protective effect on the liver cells of ALF mice and promoted the regeneration of liver cells. Subsequently, the expression and secretion levels of inflammatory and apoptotic genes in the liver were further assessed. Notably, the results showed that after transplantation of LOs and vLMs, the expression of pro-inflammatory genes (*IL-6*, *TNF-α*, *IL-1β*, and *CXCL10*) and apoptotic gene (*Bax*) in liver tissues was significantly reduced, while the expression of the anti-poptotic gene (*Bcl2*) was upregulated (Fig. 7G and S11). Correspondingly, the ELISA results showed that the secretion levels of IL-6 and TNF-α were significantly decreased, while the level of anti-inflammatory cytokine IL-10 was significantly increased in the vLMs group (Fig. 7H). These results indicated that the transplantation of vLMs could significantly reduce inflammatory responses and cell apoptosis in the liver of ALF mice.

4. Discussion

The burden of liver disease is continuously increasing on a global scale, and liver transplantation remains the sole therapeutic option for end-stage liver disease [28]. Regenerative medicine, aiming to repair or replace damaged liver tissue with healthy functional cells, holds great potential as an alternative treatment strategy [29]. As crucial components of liver tissue engineering, significant advancements have been made in the research of cell sources and scaffolds in recent years [30]. However, achieving graft vascularization and integration with the host vascular networks remains a challenge. In this study, ASCs-derived LOs were co-cultured with iPSCs-derived VOs to construct vLMs with vascular networks, in which the vascular microenvironment facilitated the differentiation and maturation of LOs. Notably, vLMs could formed perfusable vascular networks in vivo and exhibited enhanced liver function. Moreover, transplantation of vLMs in ALF mice significantly alleviated liver injury and reduced inflammatory responses, demonstrating a notable therapeutic effect. In summary, the potential of vLMs for liver regenerative medicine was highlighted in this work.

For the construction of liver microtissues, the functionality and availability of seed cells play a key role in determining the function and behavior of grafts in vitro and in vivo [31]. We optimized the culture medium according to the methods in previous studies [23], and the LOs induced in this study exhibited improved hepatocyte functionality, approaching that of PHHs. In addition, we demonstrated the rapid expansion capability of LOs, making it possible to provide enough cells for regenerative medicine within a short timeframe. Furthermore, our findings are in accord with recent studies indicating that LOs can maintain genetic stability after passage expansion. To date, significant advancements have been made in liver tissue engineering concerning biomaterials and tissue architecture, aiming at the construction of transplantable liver microtissues to improve the efficiency and functional performance of hepatocyte transplantation [32–34]. However, it cannot be ignored that vascularization is critical for the construction of functional liver microtissues.

The rapid development of VOs offers an approach that more closely mimics the physiological environment for the vascularization of organoids [35]. VOs possess the ability to integrate with other organoids and promote their maturation through paracrine signaling, thereby enhancing their similarity to native organs [36]. In this study, we innovatively proposed the co-culture of LOs and VOs to generate vLMs, in which the VNs enveloped the LOs to connect the scattered LOs into a liver microtissue that resembled the structure of liver lobules. Consistent with previous reports, it was also demonstrated in this study that VNs could secrete a variety of paracrine factors, particularly high concentrations of HGF, which significantly enhanced the expression of liver-specific genes expression and protein secretion of LOs [24,25,37]. Meanwhile, the transcriptomic sequencing of mLOs further confirmed that vascular paracrine promoted the differentiation of LOs. KEGG and GSEA enrichment analyses showed that the upregulated genes in mLOs were mainly involved in the Wnt, TGF-β, and PPAR signaling pathways, among which Wnt signaling was particularly significant, as it regulates various biological processes during development, including cell proliferation, migration, and differentiation [38]. A study on organotypic models that investigated the interaction between hepatocytes and endothelial cells suggested that increased PPARα signaling could lead to downstream effects, including the induction of cholesterol and bile acid biosynthesis as well as the enhancement of fatty acid metabolism [39].

When transplanted in vivo as functional liver microtissues, vLMs could integrate into host and connect with host blood vessels, showing higher transplantation efficiency and liver functions. Moreover, it was found that the transplantation of vLMs could effectively ameliorate the inflammatory response and promote recovery of liver in ALF mice, demonstrating superior therapeutic effects compared to LOs transplantation. On the one hand, hepatocytes within vLMs exhibited enhanced secretory and metabolic functions. On the other hand, the vascular network in vLMs accelerated the transport of nutrients and the clearance of metabolic wastes. These results indicated that vLMs, as a novel graft, possessed significant potential for clinical application in the field of liver regenerative medicine.

However, there are still several limitations need to be addressed in future research. Firstly, Matrigel was selected for organoid culture in this study because it is currently the most commonly used material due to its biocompatibility and cell adhesion properties. But we acknowledge

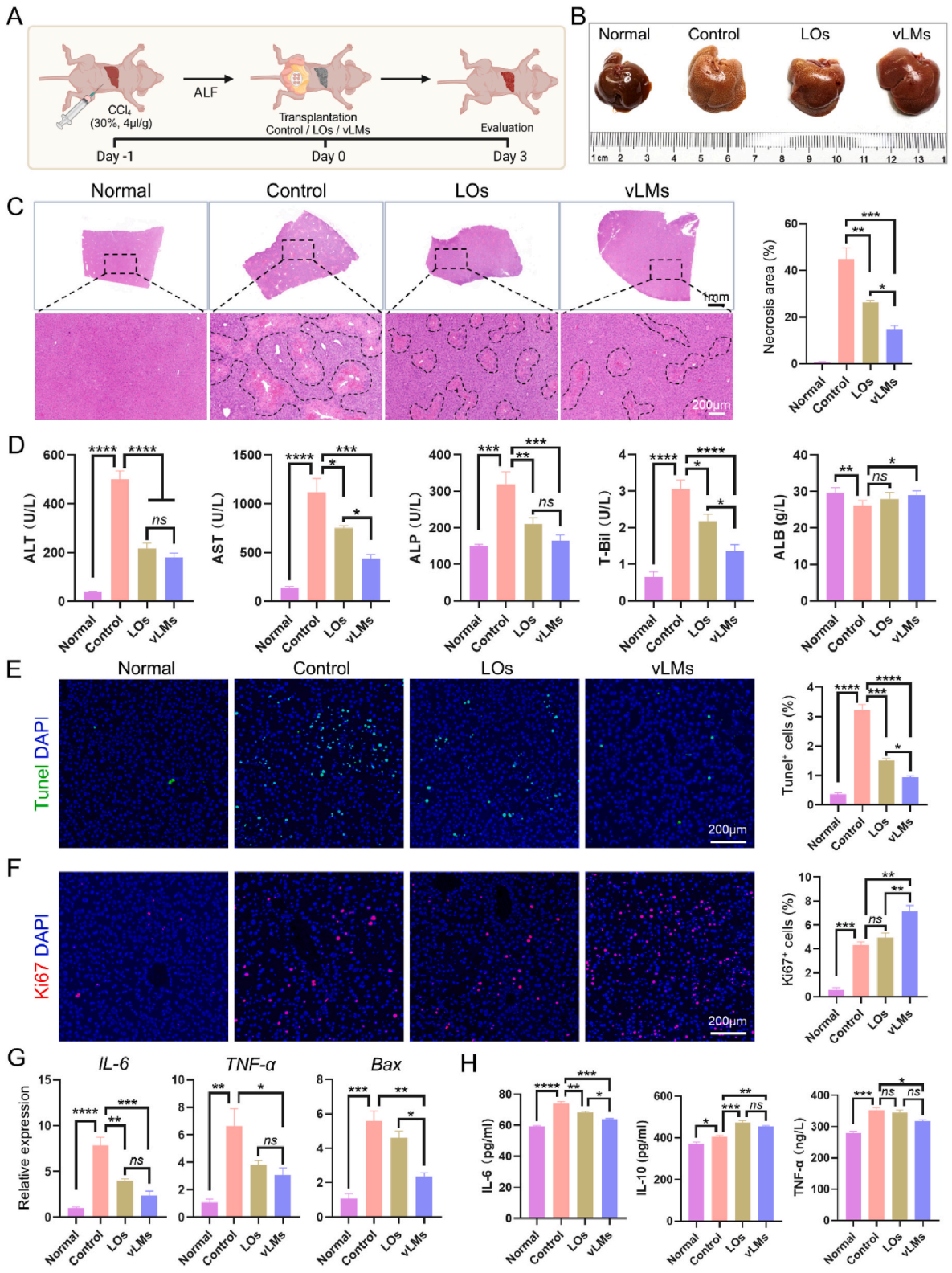

Fig. 7. Evaluation of the therapeutic effects of vLMs transplantation on CCl_4-induced ALF. (A) Schematic diagram of the experimental procedure for transplantation therapy in CCl_4-induced ALF mice. (B) Liver images of normal and ALF mice following different treatments. (C) Representative H&E staining images of mice livers with different treatments and quantitative analysis of the necrosis area. The black dashed lines indicate the necrotic areas. (D) The levels of ALT, AST, ALP, T-Bil, and ALB in serum of mice with different treatments. (E) Representative Tunel staining images of mice livers with different treatments and quantitative analysis of $Tunel^+$ cells. (F) Representative Ki67 staining images of mice livers with different treatments and quantitative analysis of $Ki67^+$ cells. (G) The relative mRNA expression levels of genes related to inflammation (*IL-6* and *TNF-α*) and apoptosis (*Bax*). (H) The secretion levels of inflammatory factors (IL-1β, IL-10, and TNF-α) in the serum of mice. Data are represented as mean ± SEM (n = 3). $^*p < 0.05$, $^{**}p < 0.01$, $^{***}p < 0.001$, $^{****}p < 0.0001$, ns: no significant difference.

its limitations in clinical translation due to animal origin, potential immunogenicity and batch-to-batch variability [40]. In recent years, bioactive materials such as biological hydrogels based on natural extracellular matrix components or hybrid-modified synthetic hydrogels have developed rapidly [41]. Future research should further explore and optimize materials for liver tissue engineering, thereby advancing clinical translation. Additionally, LOs derived from primary hepatocytes exhibit enhanced hepatic functionality, and can be used as a cell source for liver tissue engineering after further improving their amplification capacity [42]. Notably, patient-derived LOs could be combined with bio-scaffolds to generate custom engineered vLMs for autologous transplantation, thereby minimizing immune rejection responses and making it more possible to be put into clinical use.

5. Conclusion

In conclusion, our study developed functional liver microtissues from vLMs with vascular networks by fusing ASCs-derived LOs and iPSCs-derived VOs. The vascular microenvironment promoted the differentiation and maturation of LOs. The vLMs demonstrated improved liver function after transplantation in vivo, establishing connections with the recipient vasculature. Furthermore, the transplantation of vLMs could significantly alleviate liver injury and inflammatory responses, reduce apoptosis while promoting cell proliferation in CCl_4-induced ALF mice. These above results indicated that vLMs possessed a notable therapeutic efficacy for ALF and held great potential for clinical research in the field of liver regenerative medicine.

CRediT authorship contribution statement

Liuyang Zhu: Writing – original draft, Visualization, Validation, Methodology, Formal analysis. **Sen Liu:** Writing – original draft, Visualization, Validation, Formal analysis, Data curation. **Zhuangzhuang Yang:** Visualization, Validation, Investigation, Formal analysis, Data curation. **Long Yang:** Visualization, Validation, Methodology, Formal analysis. **Yueyue Yang:** Software, Methodology. **Pinsheng Han:** Methodology, Investigation, Formal analysis. **Yu Miao:** Methodology, Investigation. **Lei Lin:** Validation, Investigation. **Lilin Xu:** Investigation, Data curation. **Yan Li:** Methodology, Investigation. **Xinyue Li:** Methodology. **Libo Wang:** Visualization, Software. **Tianyu Zhao:** Software, Methodology. **Weiwei Wang:** Methodology, Investigation. **Zilin Cui:** Investigation. **Ze Wang:** Writing – review & editing, Supervision, Resources, Data curation. **Deling Kong:** Supervision, Project administration, Conceptualization. **Zhongyang Shen:** Writing – review & editing, Supervision, Project administration, Conceptualization. **Yamin Zhang:** Writing – review & editing, Supervision, Project administration, Funding acquisition, Conceptualization.

Data availability

The data that support the findings of this study are available from the corresponding author upon reasonable request. The raw data of RNA-seq datasets in this study have been deposited in the NCBI Sequence Read Archive, accession number: PRJNA1113135 and PRJNA1189691.

Ethics approval and consent to participate

All animal experiments have been approved by the Animal Experiments Ethical Committee of Nankai University (2022-SYDWLL-000189). The Medical Ethics Committee of Tianjin First Central Hospital approved the use of human samples for this study (2020N221KY), and informed consent was obtained from all the patients.

Declaration of competing interest

The authors declare that they have no known competing financial interests or personal relationships that could have appeared to influence the work reported in this paper.

Acknowledgements

This work was supported by the National Key Technologies Research and Development Program of China (2020YFA0803700), National Natural Science Foundation of China (82372194, 82204546, and 823B2049), the Tianjin Health Science and Technology Project (TJWJ2023QN034 and TJWJ2023QN028), Tianjin Natural Science Foundation (24JCYBJC01840), and Project of State Key Laboratory of Druggability Evaluation and Systematic Translational Medicine (712023001, 712023002, and 712024001).

Appendix A. Supplementary data

Supplementary data to this article can be found online at https://doi.org/10.1016/j.bioactmat.2025.04.030.

References

[1] L. Campana, H. Esser, M. Huch, S. Forbes, Liver regeneration and inflammation: from fundamental science to clinical applications, Nat. Rev. Mol. Cell Biol. 22 (9) (2021) 608–624.
[2] R. Moreau, B. Gao, M. Papp, R. Bañares, P.S. Kamath, Acute-on-chronic liver failure: a distinct clinical syndrome, J. Hepatol. 75 (Suppl 1) (2021) S27–S35, https://doi.org/10.1016/j.jhep.2020.11.047.
[3] R. Maiwall, A.V. Kulkarni, J.P. Arab, et al., Acute liver failure, Lancet 404 (10454) (2024) 789–802, https://doi.org/10.1016/S0140-6736(24)00693-7.
[4] B. Vasavada, Living-donor liver transplant for patients with end-stage liver disease, JAMA Surg. 158 (2023) 427, https://doi.org/10.1001/jamasurg.2022.7000.
[5] J. Zhang, X. Zhao, L. Liang, J. Li, U. Demirci, S. Wang, A decade of progress in liver regenerative medicine, Biomaterials 157 (2018) 161–176, https://doi.org/10.1016/j.biomaterials.2017.11.027.
[6] D. Huang, S.B. Gibeley, C. Xu, Y. Xiao, O. Celik, H.N. Ginsberg, K.W. Leong, Engineering liver microtissues for disease modeling and regenerative medicine, Adv. Funct. Mater. 30 (2020) 1909553, https://doi.org/10.1002/adfm.201909553 [pii].
[7] J. Zhang, X. Chen, Y. Chai, et al., 3D printing of a vascularized mini-liver based on the size-dependent functional enhancements of cell spheroids for rescue of liver failure, Adv. Sci. 11 (17) (2024) e2309899, https://doi.org/10.1002/advs.202309899.
[8] J. Zhang, H.F. Chan, H. Wang, et al., Stem cell therapy and tissue engineering strategies using cell aggregates and decellularized scaffolds for the rescue of liver failure, J. Tissue Eng. 12 (2021) 2041731420986711, https://doi.org/10.1177/2041731420986711.
[9] Z. Heydari, M. Najimi, H. Mirzaei, A. Shpichka, M. Ruoss, Z. Farzaneh, L. Montazeri, A. Piryaei, P. Timashev, R. Gramignoli, et al., Tissue engineering in liver regenerative medicine: insights into novel translational technologies, Cells 9 (2020) 304, https://doi.org/10.3390/cells9020304.
[10] N. Prior, P. Inacio, M. Huch, Liver organoids: from basic research to therapeutic applications, Gut 68 (2019) 2228–2237, https://doi.org/10.1136/gutjnl-2019-319256.
[11] S. Liu, C. Cheng, L. Zhu, T. Zhao, Z. Wang, X. Yi, F. Yan, X. Wang, C. Li, T. Cui, et al., Liver organoids: updates on generation strategies and biomedical applications, Stem Cell Res. Ther. 15 (2024) 244, https://doi.org/10.1186/s13287-024-03865-3.
[12] M. Huch, H. Gehart, R. van Boxtel, K. Hamer, F. Blokzijl, M.M. Verstegen, E. Ellis, M. van Wenum, S.A. Fuchs, J. de Ligt, et al., Long-term culture of genome-stable bipotent stem cells from adult human liver, Cell 160 (2015) 299–312, https://doi.org/10.1016/j.cell.2014.11.050.
[13] S.J. Mun, J.S. Ryu, M.O. Lee, Y.S. Son, S.J. Oh, H.S. Cho, M.Y. Son, D.S. Kim, S. J. Kim, H.J. Yoo, et al., Generation of expandable human pluripotent stem cell-derived hepatocyte-like liver organoids, J. Hepatol. 71 (2019) 970–985, https://doi.org/10.1016/j.jhep.2019.06.030.
[14] S. Wang, X. Wang, Z. Tan, Y. Su, J. Liu, M. Chang, F. Yan, J. Chen, T. Chen, C. Li, et al., Human ESC-derived expandable hepatic organoids enable therapeutic liver repopulation and pathophysiological modeling of alcoholic liver injury, Cell Res. 29 (2019) 1009–1026, https://doi.org/10.1038/s41422-019-0242-8.
[15] H.J. Kim, G. Kim, K.Y. Chi, J.H. Kim, In vitro generation of luminal vasculature in liver organoids: from basic vascular biology to vascularized hepatic organoids, Int J Stem Cells 16 (2023) 1–15, https://doi.org/10.15283/ijsc22154.
[16] T. Takebe, R.R. Zhang, H. Koike, M. Kimura, E. Yoshizawa, M. Enomura, N. Koike, K. Sekine, H. Taniguchi, Generation of a vascularized and functional human liver from an iPSC-derived organ bud transplant, Nat. Protoc. 9 (2014) 396–409, https://doi.org/10.1038/nprot.2014.020.
[17] K.K. Yap, Y.W. Gerrand, A.M. Dingle, G.C. Yeoh, W.A. Morrison, G.M. Mitchell, Liver sinusoidal endothelial cells promote the differentiation and survival of mouse vascularised hepatobiliary organoids, Biomaterials 251 (2020) 120091, https://doi.org/10.1016/j.biomaterials.2020.120091.

[18] F. Li, H. Wei, Y. Jin, et al., Microfluidic fabrication of MicroRNA-induced hepatocyte-like cells/human umbilical vein endothelial cells-laden microgels for acute liver failure treatment, ACS Nano 17 (24) (2023) 25243–25256, https://doi.org/10.1021/acsnano.3c08495.
[19] R.A. Wimmer, A. Leopoldi, M. Aichinger, D. Kerjaschki, J.M. Penninger, Generation of blood vessel organoids from human pluripotent stem cells, Nat. Protoc. 14 (2019) 3082–3100, https://doi.org/10.1038/s41596-019-0213-z.
[20] K. Salewskij, J.M. Penninger, Blood vessel organoids for development and disease, Circ. Res. 132 (2023) 498–510, https://doi.org/10.1161/CIRCRESAHA.122.321768.
[21] Y. Ahn, J.H. An, H.J. Yang, D.G. Lee, J. Kim, H. Koh, Y.H. Park, B.S. Song, B. W. Sim, H.J. Lee, et al., Human blood vessel organoids penetrate human cerebral organoids and form a vessel-like system, Cells 10 (2021) 2036, https://doi.org/10.3390/cells10082036.
[22] X.Y. Sun, X.C. Ju, Y. Li, P.M. Zeng, J. Wu, Y.Y. Zhou, L.B. Shen, J. Dong, Y.J. Chen, Z.G. Luo, Generation of vascularized brain organoids to study neurovascular interactions, Elife 11 (2022) e76707, https://doi.org/10.7554/eLife.76707.
[23] Y. Hu, X. Hu, J. Luo, J. Huang, Y. Sun, H. Li, Y. Qiao, H. Wu, J. Li, L. Zhou, et al., Liver organoid culture methods, Cell Biosci. 13 (2023) 197, https://doi.org/10.1186/s13578-023-01136-x.
[24] A.M. Dingle, K.K. Yap, Y.W. Gerrand, C.J. Taylor, E. Keramidaris, Z. Lokmic, A. M. Kong, H.L. Peters, W.A. Morrison, G.M. Mitchell, Characterization of isolated liver sinusoidal endothelial cells for liver bioengineering, Angiogenesis 21 (2018) 581–597, https://doi.org/10.1007/s10456-018-9610-0.
[25] T. Leibing, C. Géraud, I. Augustin, M. Boutros, H.G. Augustin, J.G. Okun, C. D. Langhans, J. Zierow, S.A. Wohlfeil, V. Olsavszky, et al., Angiocrine Wnt signaling controls liver growth and metabolic maturation in mice, Hepatology 68 (2018) 707–722, https://doi.org/10.1002/hep.29613.
[26] J.B. Pan, S.C. Hu, D. Shi, M.C. Cai, Y.B. Li, Q. Zou, Z.L. Ji, PaGenBase: a pattern gene database for the global and dynamic understanding of gene function, PLoS One 8 (2013) e80747, https://doi.org/10.1371/journal.pone.0080747.
[27] W.C. Peng, C.Y. Logan, M. Fish, T. Anbarchian, F. Aguisanda, A. Álvarez-Varela, P. Wu, Y. Jin, J. Zhu, B. Li, et al., Inflammatory cytokine TNFα promotes the long-term expansion of primary hepatocytes in 3D culture, Cell 175 (2018) 1607–1619. e15, https://doi.org/10.1016/j.cell.2018.11.012.
[28] T. Hibi, A.K. Wei Chieh, A. Chi-Yan Chan, P. Bhangui, Current status of liver transplantation in Asia, Int. J. Surg. 82S (2020) 4–8, https://doi.org/10.1016/j.ijsu.2020.05.071.
[29] V. Cardinale, N. Lanthier, P.M. Baptista, G. Carpino, G. Carnevale, G. Orlando, R. Angelico, T.M. Manzia, D. Schuppan, M. Pinzani, et al., Cell transplantation-based regenerative medicine in liver diseases, Stem Cell Rep. 18 (2023) 1555–1572, https://doi.org/10.1016/j.stemcr.2023.06.005.
[30] M. Luo, J. Lai, E. Zhang, Y. Ma, R. He, L. Mao, B. Deng, J. Zhu, Y. Ding, J. Huang, et al., Rapid self-assembly mini-livers protect mice against severe hepatectomy-induced liver failure, Adv. Sci. 11 (2024) e2309166, https://doi.org/10.1002/advs.202309166.
[31] W. Lv, H. Zhou, A. Aazmi, et al., Constructing biomimetic liver models through biomaterials and vasculature engineering, Regen. Biomater. 9 (2022) rbac079, https://doi.org/10.1093/rb/rbac079.
[32] H.A. Reza, R. Okabe, T. Takebe, Organoid transplant approaches for the liver. Transpl, Int 34 (2021) 2031–2045, https://doi.org/10.1111/tri.14128.
[33] G. Li, J. He, J. Shi, et al., Bioprinting functional hepatocyte organoids derived from human chemically induced pluripotent stem cells to treat liver failure, Gut (2025), https://doi.org/10.1136/gutjnl-2024-333885 gutjnl-2024-333885 [pii].
[34] J. Zhang, X. Chen, Y. Chai, et al., Mesenchymal stromal/stem cell spheroid-derived extracellular vesicles advance the therapeutic efficacy of 3D-printed vascularized artificial liver lobules in liver failure treatment, Bioact. Mater. 49 (2025) 121–139, https://doi.org/10.1016/j.bioactmat.2025.02.042.
[35] H. Naderi-Meshkin, V.A. Cornelius, M. Eleftheriadou, K.N. Potel, W. Setyaningsih, A. Margariti, Vascular organoids: unveiling advantages, applications, challenges, and disease modelling strategies, Stem Cell Res. Ther. 14 (2023) 292, https://doi.org/10.1186/s13287-023-03521-2.
[36] H.S. Roh, D.E. Kim, G. Kim, J. Kim, D. Fan, H.S. Kim, Y.H. Kim, J.H. Lee, B.G. Kim, M.O. Ryu, et al., Establishment and long-term expansion of adult hepatobiliary organoids co-cultured with liver endothelial cells, Heliyon 10 (2024) e36120, https://doi.org/10.1016/j.heliyon.2024.e36120.
[37] D. Nam, M.R. Park, H. Lee, et al., Induced endothelial cell-integrated liver assembloids promote hepatic maturation and therapeutic effect on cholestatic liver fibrosis, Cells 11 (14) (2022) 2242, https://doi.org/10.3390/cells11142242.
[38] B.S. Ding, D.J. Nolan, J.M. Butler, et al., Inductive angiocrine signals from sinusoidal endothelium are required for liver regeneration, Nature 468 (7321) (2010) 310–315, https://doi.org/10.1038/nature09493.
[39] A.N. Tegge, R.R. Rodrigues, A.L. Larkin, L. Vu, T.M. Murali, P. Rajagopalan, Transcriptomic analysis of hepatic cells in multicellular organotypic liver models, Sci. Rep. 8 (2018) 11306, https://doi.org/10.1038/s41598-018-29455-x.
[40] M.T. Kozlowski, C.J. Crook, H.T. Ku, Towards organoid culture without Matrigel, Commun. Biol. 4 (2021) 1387, https://doi.org/10.1038/s42003-021-02910-8.
[41] Z. Gan, X. Qin, H. Liu, J. Liu, J. Qin, Recent advances in defined hydrogels in organoid research, Bioact. Mater. 28 (2023) 386–401, https://doi.org/10.1016/j.bioactmat.2023.06.004.
[42] D. Hendriks, B. Artegiani, T. Margaritis, I. Zoutendijk, S. Chuva de Sousa Lopes, H. Clevers, Mapping of mitogen and metabolic sensitivity in organoids defines requirements for human hepatocyte growth, Nat. Commun. 15 (2024) 4034, https://doi.org/10.1038/s41467-024-48550-4.